J Mater Sci (2007) 42:8824–8837
DOI 10.1007/s10853-007-1859-4



# Micromechanics of crystal interfaces in polycrystalline solid phases of porous media: fundamentals and application to strength of hydroxyapatite biomaterials

**Andreas Fritsch · Luc Dormieux · Christian Hellmich · Julien Sanahuja**

Received: 20 February 2007 / Accepted: 17 May 2007 / Published online: 7 August 2007


**Abstract** Interfaces are often believed to play a role in the mechanical behavior of mineralized biological and biomimetic materials. This motivates the micromechanical description of the elasticity and brittle failure of interfaces between crystals in a (dense) polycrystal, which serves as the skeleton of a porous material defined one observation scale above. Equilibrium and compatibility conditions, together with a suitable matrix-inclusion problem with a compliant interface, yield the homogenized elastic properties of the polycrystal, and of the porous material with polycrystalline solid phase. Incompressibility of single crystals guarantees finite shear stiffness of the polycrystal, even for vanishing interface stiffness, while increasing the latter generally leads to an increase of polycrystal shear stiffness. Corresponding elastic energy expressions give access to effective stresses representing the stress heterogeneities in the microstructures, which induce brittle failure. Thereby, Coulomb-type brittle failure of the crystalline interfaces implies Drucker–Prager-type (brittle, elastic limit-type) failure properties at the scale of the polycrystal. At the even higher scale of the porous material, high interfacial rigidities or low interfacial friction angles may result in closed elastic domains, indicating material failure even under hydrostatic pressure. This micromechanics model can satisfactorily reproduce the experimental strength data of different (brittle) hydroxyapatite biomaterials, across largely variable porosities. Thereby, the brittle failure criteria can be well approximated by micromechanically derived criteria referring to ductile solid matrices, both criteria being even identical if the solid matrix is incompressible.

Andreas Fritsch—On leave from Institute for Mechanics of Materials and Structures, Vienna University of Technology (TU Wien), 1040 Vienna, Austria.

A. Fritsch · L. Dormieux
Laboratory of Materials and Structures, National School of Civil Engineering (ENPC), Marne-la-Vallee 77455, France

A. Fritsch
e-mail: Andreas.Fritsch@tuwien.ac.at

L. Dormieux
e-mail: dormieux@lmsgc.enpc.fr

C. Hellmich (✉)
Institute for Mechanics of Materials and Structures, Vienna University of Technology (TU Wien), Vienna 1040, Austria
e-mail: Christian.Hellmich@tuwien.ac.at

J. Sanahuja
Lafarge Research Center, Saint-Quentin Fallavier Cedex 38291, France
e-mail: julien.sanahuja@lafarge.com

## Introduction

Interfaces are believed to often play a fundamental role in the mechanical behavior of hierarchically organized biological materials. Accordingly, much attention has been paid to the polymer-filled interfaces between ceramic tablets in nacre [2, 20, 32, 33, 39, 40, 41], but the importance of interfacial behavior was also discussed for other classes of biological materials, such as bone [48].

To gain insight into these material systems, material/microstructure models have been developed within different theoretical frameworks, such as fracture mechanics and scaling laws [20, 39, 40, 41], large-scale elastoplastic Finite Element analyses [32, 33, 48], or periodic homogenization on the basis of a unit cell discretized by Finite Elements [2].

In addition to such periodic, FE-based ('computational') homogenization approaches, analytical and/or semianalytical approaches of random homogenization (continuum micromechanics [51, 52]) have been recently used as to effectively predict the elastic properties of complicated hierarchically structured material systems (such as bone [19, 22, 24, 25], wood [29, 30], concrete [5, 23, 49], or shale [50]), from the elasticity and the mechanical interactions—over different observation scales—of nanoscaled elementary components. Thereby, not every single detail of the highly random microstructures, but only the essential morphological features are considered, in terms of homogeneous subdomains (material phases) inside representative volume elements (RVEs, Fig. 1), their volume fractions, their elasticity, and their mechanical interaction. Theoretically, it has been recently well understood how to extend these homogenization techniques to the *ductile* failure of (*bulk*) phases [3, 4, 6, 10, 12, 15] (while applications to real materials [37] are more rare than for the elastic case). In comparison, the treatment of *brittle* failure and of *interfaces* in the framework of random homogenization is still a very open field: It is the focus of this paper—both fundamentally, and in view of the failure of biomimetic hydroxyapatite biomaterials.

Extending very recent results [14, 44], where inclusion coatings and interfaces in porous polycrystals were modeled, we here tackle the description of the elasticity and failure of interfaces between crystals in a (dense) polycrystal, which serves as the skeleton of a porous material defined one observation scale above (Fig. 2). Thereby, we

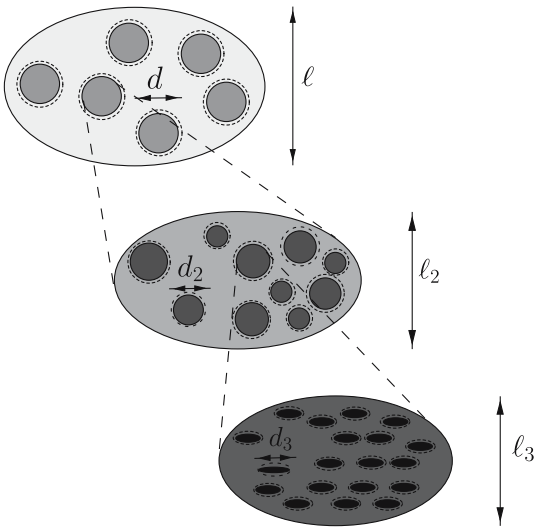


**Fig. 1** Multistep homogenization: properties of phases (with characteristic lengths of $d$ and $d_2$, respectively) inside RVEs with characteristic lengths of $\ell$ or $\ell_2$, respectively, are determined from homogenization over smaller RVEs with characteristic lengths of $\ell_2 \leq d$ and $\ell_3 \leq d_2$, respectively

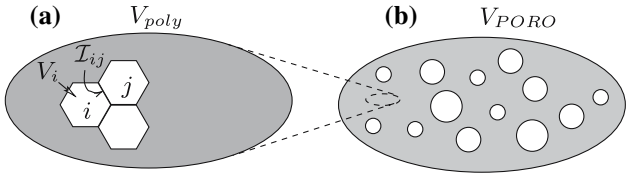


**Fig. 2** (**a**) Polycrystal with interfaces (schematic representation of volume $V_i$ of crystal $i$ and interface $\mathcal{I}_{ij}$ between crystals $i$ and $j$), serving as skeleton in a porous material at larger observation scale (**b**)

show characteristic features of a corresponding new micromechanics model, which is based on matrix-inclusion problems with compliant interfaces [21, 27, 53], and which turns out to reasonably explain the behavior of porous hydroxyapatite biomaterials, especially for their brittle failure in the compressive regime.

## Fundamentals of continuum micromechanics—representative volume element

In continuum micromechanics [28, 47, 51, 52], a material is understood as a macro-homogeneous, but micro-heterogeneous body filling a representative volume element (RVE) with characteristic length $\ell, \ell \gg d, d$ standing for the characteristic length of inhomogeneities within the RVE (see Fig. 1), and $\ell \ll \mathcal{L}, \mathcal{L}$ standing for the characteristic lengths of geometry or loading of a structure built up by the material defined on the RVE (see Table 1 for a list of all symbols in this paper). In general, the microstructure within one RVE is so complicated that it cannot be described in complete detail. Therefore, quasi-homogeneous subdomains with known physical quantities (such as volume fractions or elastic properties) are reasonably chosen. They typically include 3D subdomains, and may also include the 2D interfaces between the 3D subdomains. They are called material phases; bulk and interface phases, respectively. The 'homogenized' mechanical behavior of the overall material, i.e., the relation between homogeneous deformations acting on the boundary of the RVE and resulting (average) stresses, or the ultimate stresses sustainable by the RVE, can then be estimated from the mechanical behavior of the aforementioned homogeneous phases (representing the inhomogeneities within the RVE), their dosages within the RVE, their characteristic shapes, and their interactions. If a single phase exhibits a heterogeneous microstructure itself, its mechanical behavior can be estimated by introduction of an RVE within this phase, with dimensions $\ell_2 \leq d$, comprising again smaller phases with characteristic length $d_2 \ll \ell_2$, and so on, leading to a multistep homogenization scheme (see Fig. 1).

**Table 1** List of symbols

| | |
|---|---|
| $A_C$ | Surface area of spherical crystal with radius $a$ |
| $A_{\mathrm{ex}}$ | Constant in solution of matrix-inclusion problem with compliant interface |
| $A_i$ | Surface area of crystal $i$ |
| $A_{\mathrm{in}}$ | Constant in solution of matrix-inclusion problem with compliant interface |
| $a$ | Characteristic crystal radius |
| $B_{\mathrm{ex}}$ | Constant in solution of matrix-inclusion problem with compliant interface |
| $B_{\mathrm{in}}$ | Constant in solution of matrix-inclusion problem with compliant interface |
| $C_{\mathrm{ex}}$ | Constant in solution of matrix-inclusion problem with compliant interface |
| $\mathbb{C}_C$ | Fourth-order stiffness tensor of single crystals within the RVE $V_{\mathrm{poly}}$ |
| $\mathbb{C}_{\mathrm{poly}}$ | Fourth-order homogenized stiffness tensor of polycrystal with compliant interfaces |
| $\mathbb{C}_{\mathrm{PORO}}$ | Fourth-order homogenized stiffness tensor of a porous material the solid phase of which is a polycrystal with weak interfaces |
| $d$ | Characteristic length of inhomogeneities within the RVE |
| $\boldsymbol{E}_{\mathrm{poly}}$ | Second-order 'macroscopic' strain tensor (related to RVE $V_{\mathrm{poly}}$ of polycrystal with compliant interfaces) |
| $\boldsymbol{E}_0$ | Uniform strain imposed at infinity of matrix surrounding inclusion with compliant interface |
| $E_{\mathrm{poly,v}}$ | 'Macroscopic' volumetric strain (related to RVE $V_{\mathrm{poly}}$ of polycrystal with compliant interfaces) |
| $E_{\mathrm{poly,d}}$ | 'Macroscopic' equivalent deviatoric strain (related to RVE $V_{\mathrm{poly}}$ of polycrystal with compliant interfaces) |
| $\underline{e}_r$ | Radial unit vector |
| $\underline{e}_1, \underline{e}_2, \underline{e}_3$ | Unit base vectors of Cartesian base frame |
| $f_i$ | Volume fraction of crystal $i$ within the RVE $V_{\mathrm{poly}}$ |
| $h$ | Cohesion of interfaces between single crystals |
| $\mathbb{I}$ | Fourth-order identity tensor |
| $\mathcal{I}$ | Entity of interfaces within polycrystalline RVE $V_{\mathrm{poly}}$ |
| $\mathcal{I}_{ij}$ | Interface between crystals $i$ and $j$ |
| $\mathbb{J}$ | Volumetric part of fourth-order identity tensor $\mathbb{I}$ |
| $\mathbb{K}$ | Deviatoric part of fourth-order identity tensor $\mathbb{I}$ |
| $\boldsymbol{K}$ | Second-order interface stiffness tensor |
| $\boldsymbol{K}' = 2\boldsymbol{K}$ | Second-order interface stiffness tensor in matrix-inclusion problem with compliant interface |
| $K_n$ | Normal interface stiffness (component of $\boldsymbol{K}$) |
| $K_t$ | Tangential interface stiffness (component of $\boldsymbol{K}$) |
| $k_C$ | Bulk modulus of single crystals |
| $k_{\mathrm{poly}}$ | Homogenized bulk modulus of polycrystal with compliant interfaces (RVE $V_{\mathrm{poly}}$) |
| $k_{\mathrm{PORO}}$ | Homogenized bulk modulus of a porous material the solid phase of which is a polycrystal with compliant interfaces |
| $\ell$ | Characteristic length of the RVE |
| $\mathcal{L}$ | Characteristic lengths of geometry or loading of a structure built up by the material defined on the RVE |
| $\underline{n}$ | Normal vector onto surface of a single crystal |
| RVE | Representative volume element |

**Table 1** continued

| | |
|---|---|
| $r$ | Radial coordinate in spherical coordinate system |
| $\mathbb{S}$ | Fourth-order Eshelby tensor for spherical inclusions |
| $\underline{T}$ | Traction force vector acting on surface element of interface |
| $T_n$ | Normal component of $\underline{T}$ |
| $T_t$ | Tangential component of $\underline{T}$ |
| $T_t^{\mathrm{cr}}$ | Critical (maximum) tangential traction bearable by intercrystalline interface |
| $\underline{t}$ | Tangential vector to surface of a single crystal |
| tr | Trace of a second-order tensor |
| $V_C$ | Volume of spherical crystal with radius $a$ |
| $\partial V_C$ | Surface of spherical crystal with radius $a$ |
| $V_i$ | Volume of crystal $i$ |
| $\partial V_i$ | Surface of crystal $i$ |
| $V_{\mathrm{poly}}$ | Volume of an RVE of polycrystal with compliant interfaces |
| $V_{\mathrm{PORO}}$ | Volume of an RVE of porous material the solid phase of which is a polycrystal with compliant interfaces |
| $V_S$ | Volume of solid phase within the RVE $V_{\mathrm{PORO}}$ |
| $\underline{x}$ | Position vector within an RVE, either $V_{\mathrm{poly}}$ or $V_{\mathrm{PORO}}$ |
| $\alpha$ | Friction angle of interfaces between single crystals |
| $\delta_{ij}$ | Kronecker delta (components of second-order identity tensor $\mathbf{1}$) |
| $\delta_{\mathcal{I}}$ | Dirac distribution supported on $\mathcal{I}$ |
| $\boldsymbol{\varepsilon}$ | Second-order strain tensor field within single crystals filling RVE $V_{\mathrm{poly}}$ of polycrystal with compliant interfaces |
| $\theta$ | Latitudinal coordinate of spherical coordinate system |
| $\kappa = K_t' a/\mu_C$ | Dimensionless quantity related to rigidity of interface |
| $\mu_C$ | Shear modulus of single crystals |
| $\mu_{\mathrm{poly}}$ | Homogenized shear modulus of polycrystal with compliant interfaces (RVE $V_{\mathrm{poly}}$) |
| $\mu_{\mathrm{PORO}}$ | Homogenized shear modulus of a porous material the solid phase of which is a polycrystal with compliant interfaces |
| $\nu_{\mathrm{poly}}$ | Homogenized Poisson's ratio of polycrystal with compliant interfaces (RVE $V_{\mathrm{poly}}$) |
| $\underline{\xi}$ | Displacements within and at the boundary of RVE $V_{\mathrm{poly}}$ |
| $[\![\underline{\xi}]\!]$ | Displacement discontinuity at the interfaces between crystals |
| $[\![\xi_n]\!]$ | Normal component of $[\![\underline{\xi}]\!]$ |
| $[\![\xi_t]\!]$ | Tangential component of $[\![\underline{\xi}]\!]$ |
| $[\underline{\xi}]$ | Displacement discontinuity at compliant interface of 'generalized' matrix-inclusion problem |
| $\underline{\xi}_i, \underline{\xi}_j$ | Displacements along interface $\mathcal{I}_{ij}$, in crystal $i$ and $j$, respectively |
| $\overline{\underline{\xi}}$ | Mean displacement at the interface $\mathcal{I}_{ij}$ |
| $\underline{\xi}_{\mathrm{in}}$ | Displacement field inside the inclusion surrounded by compliant interface and infinite matrix (related to 'generalized' matrix-inclusion problem) |
| $\underline{\xi}_{\mathrm{ex}}$ | Displacement field throughout the matrix surrounding inclusion coated by compliant interface (related to 'generalized' matrix-inclusion problem) |

**Table 1** continued

| | |
|---|---|
| $\boldsymbol{\Sigma}_{\text{poly}}$ | Second-order 'macroscopic' stress tensor (related to RVE $V_{\text{poly}}$ of polycrystal with weak interfaces) |
| $\Sigma_{\text{poly},m}$ | 'Macroscopic' mean stress (related to RVE $V_{\text{poly}}$ of polycrystal with weak interfaces) |
| $\Sigma_{\text{poly},d}$ | 'Macroscopic' equivalent deviatoric stress (related to RVE $V_{\text{poly}}$ of polycrystal with weak interfaces) |
| $\boldsymbol{\Sigma}_{\text{PORO}}$ | Second-order macroscopic stress tensor (related to RVE $V_{\text{PORO}}$ of porous material the solid phase of which is a polycrystal with weak interfaces) |
| $\Sigma_{\text{PORO},m}$ | Macroscopic mean stress (related to RVE $V_{\text{PORO}}$ of porous material the solid phase of which is a polycrystal with weak interfaces) |
| $\Sigma_{\text{PORO},d}$ | Macroscopic equivalent deviatoric stress (related to RVE $V_{\text{PORO}}$ of porous material the solid phase of which is a polycrystal with weak interfaces) |
| $\boldsymbol{\sigma}$ | Second-order stress tensor field with in single crystals filling RVE $V_{\text{poly}}$ of polycrystal with compliant interfaces |
| $\boldsymbol{\sigma}_{\text{in}}$ | Stress field inside the inclusion surrounded by compliant interface and infinite matrix (related to 'generalized' matrix-inclusion problem) |
| $\boldsymbol{\sigma}_{\text{ex}}$ | Stress field throughout the matrix surrounding inclusion coated by compliant interface (related to 'generalized' matrix-inclusion problem) |
| $\sigma$ | Scattering factor in two-membered evolution strategy |
| $\phi$ | Longitudinal coordinate of spherical coordinate system |
| $\varphi$ | Volume fraction of pores within the RVE $V_{\text{PORO}}$ |
| $\chi = \mu_C/k_C$ | Dimensionless quantity related to compressibility of single crystals |
| $\Psi$ | Macroscopic energy density |
| $\mathbf{1}$ | Second-order identity tensor |
| $\cdot$ | First-order tensor contraction |
| : | Second-order tensor contraction |
| $\otimes$ | Dyadic product of tensors |

## Micromechanics of polycrystal with weak interfaces

### Micromechanical representation

We consider an RVE with volume $V_{\text{poly}}$ (Figs. 2a, 9a) hosting single crystals of typically quasi-spherical shape and of volume $V_i$, separated from each other by very thin (essentially 2D) interfaces $\mathcal{I}_{ij}$ between crystals $i$ and $j$, all interfaces making up the entity of interfaces $\mathcal{I}, \cup\mathcal{I}_{ij} = \mathcal{I}$, see Fig. 2. 'Macroscopic' strains $\boldsymbol{E}_{\text{poly}}$ are imposed at the boundary of the RVE $V_{\text{poly}}$ in terms of displacements $\underline{\xi}$,

$$\text{on } \partial V_{\text{poly}} : \underline{\xi}(\underline{x}) = \boldsymbol{E}_{\text{poly}} \cdot \underline{x} \tag{1}$$

with $\underline{x}$ as the position vector within the RVE. The geometrical compatibility of (1) with the local 'microscopic' strains $\boldsymbol{\varepsilon}(\underline{x})$ in the crystals and the displacement discontinuities $[\![\underline{\xi}]\!] = \underline{\xi}_j - \underline{\xi}_i$ at the interfaces $\mathcal{I}_{ij}$ between the crystals $i$ and $j$ implies [14]

$$\begin{aligned}\boldsymbol{E}_{\text{poly}} &= \frac{1}{V_{\text{poly}}}\left(\int_{V_{\text{poly}}} \boldsymbol{\varepsilon}(\underline{x})\mathrm{d}V + \sum_{ij}\int_{\mathcal{I}_{ij}} [\![\underline{\xi}]\!] \overset{s}{\otimes} \underline{n}\mathrm{d}S\right)\\ &= \frac{1}{V_{\text{poly}}}\sum_i \int_{\partial V_i} \bar{\underline{\xi}} \overset{s}{\otimes} \underline{n}\mathrm{d}S = \sum_i \frac{f_i}{V_i}\int_{\partial V_i} \bar{\underline{\xi}} \overset{s}{\otimes} \underline{n}\mathrm{d}S\end{aligned} \tag{2}$$

with location vector $\underline{x}$, normal $\underline{n}$ onto the spherical surface of the crystals,

$$\bar{\underline{\xi}} = (\underline{\xi}_i + \underline{\xi}_j)/2 = \underline{\xi}_j - [\![\underline{\xi}]\!]/2 = \underline{\xi}_i + [\![\underline{\xi}]\!]/2 \tag{3}$$

as the mean displacement at the interface $\mathcal{I}_{ij}, V_i$ and $f_i = V_i/V_{\text{poly}}$ as the volume and the volume fraction of the $i$th crystal, and $\partial V_i$ as its surface with area $A_i$. For crystals of the same shape and size (with volume $V_C$ and surface $\partial V_C$), and indiscernible average mean displacements at their surfaces, (2) can be transformed to

$$\boldsymbol{E}_{\text{poly}} = \frac{1}{V_C}\int_{\partial V_C} \bar{\underline{\xi}} \overset{s}{\otimes} \underline{n}\mathrm{d}S \tag{4}$$

The corresponding 'macroscopic' stresses $\boldsymbol{\Sigma}_{\text{poly}}$ are equal to the spatial average of the (equilibrated) local stresses $\boldsymbol{\sigma}(\underline{x})$ inside the RVE $V_{\text{poly}}$,

$$\begin{aligned}\boldsymbol{\Sigma}_{\text{poly}} &= \langle\boldsymbol{\sigma}(\underline{x})\rangle = \frac{1}{V_{\text{poly}}}\int_{V_{\text{poly}}} \boldsymbol{\sigma}(\underline{x})\mathrm{d}V\\ &= \sum_i \frac{f_i}{V_i}\int_{V_i} \boldsymbol{\sigma}(\underline{x})\mathrm{d}V\\ &= \sum_i \frac{f_i}{V_i}\int_{\partial V_i} \underline{x} \otimes [\boldsymbol{\sigma}(\underline{x}) \cdot \underline{n}(\underline{x})]\mathrm{d}S\end{aligned} \tag{5}$$

For spherical crystals with radius $a$, surface $\partial V_C$ with area $A_C = 4\pi a^2$, and volume $V_C = 4/3\pi a^3$, (5) can be further transformed,

$$\begin{aligned}\boldsymbol{\Sigma}_{\text{poly}} &= \sum_i \frac{f_i}{\frac{4}{3}\pi a^3}\int_{\partial V_C} a\underline{e}_r(\underline{x}) \otimes [\boldsymbol{\sigma}(\underline{x}) \cdot \underline{e}_r(\underline{x})]\mathrm{d}S\\ &= \sum_i \frac{3f_i}{A_C}\int_{\partial V_C} \underline{e}_r(\underline{x}) \otimes [\boldsymbol{\sigma}(\underline{x}) \cdot \underline{e}_r(\underline{x})]\mathrm{d}S\\ &= \frac{1}{V_C}\int_{\partial V_C} a\underline{n}(\underline{x}) \otimes [\boldsymbol{\sigma}(\underline{x}) \cdot \underline{n}(\underline{x})]\mathrm{d}S\\ &= \frac{3}{A_C}\int_{\partial V_C} \underline{n}(\underline{x}) \otimes [\boldsymbol{\sigma}(\underline{x}) \cdot \underline{n}(\underline{x})]\mathrm{d}S\\ &= \frac{1}{V_C}\int_{V_C} \boldsymbol{\sigma}(\underline{x})\mathrm{d}V\end{aligned} \tag{6}$$

with radial unit vector $\underline{e}_r$ being identical to the normal $\underline{n}$. Since the microscopic stresses are equilibrated (div $\boldsymbol{\sigma} = \underline{0}$), (5) and (6) imply [9, p. 118, 28], that the 'macroscopic' stresses act as traction forces $\boldsymbol{\Sigma}_{\text{poly}} \cdot \underline{n}$ both at the boundary of the RVE, $\partial V_{\text{poly}}$, and those of single crystals, $\partial V_C$,

$$\text{on } \partial V_{\text{poly}} \text{ and } \partial V_C: \quad \boldsymbol{\sigma}(\underline{x}) \cdot \underline{n}(\underline{x}) = \boldsymbol{\Sigma}_{\text{poly}} \cdot \underline{n}(\underline{x}) \tag{7}$$

The relation between $\boldsymbol{\Sigma}_{\text{poly}}$ and $\boldsymbol{E}_{\text{poly}}$ depends on the constitutive behavior of the single crystals and of the interfaces between them.

## Constitutive behavior of interfaces and single crystals

The interfaces are the weakest locations of the material, the load bearing capacities of which are bounded according to a Coulomb-type law,

$$\forall \underline{x} \in \mathcal{I}_{ij} : T_t(\underline{x}) \leq T_t^{\text{cr}} = \alpha(h - T_n(\underline{x})) \tag{8}$$

with friction angle $\alpha$, cohesion $h$, and $T_t$ and $T_n$ as the tangential and normal components of the traction force $\underline{T} = T_n\underline{n} + T_t\underline{t}$ acting on an infinitesimal interface area around $\underline{x}$, with normal $\underline{n}$, and $\underline{t}$ as the tangential unit vector, $\underline{t} \cdot \underline{n} = 0$. We consider brittle interface failure once a critical value $T_t = T_t^{\text{cr}}$ is reached in (8).

Below this critical value, the interface behaves linear elastically, i.e., the interface traction $\underline{T}(\underline{x})$ is related to a displacement discontinuity $[\![\underline{\xi}]\!](\underline{x})$ encountered when crossing the interface $\mathcal{I}_{ij}$ along $\underline{n}(\underline{x})$:

$$\begin{aligned} &\underline{T}(\underline{x}) = \boldsymbol{K} \cdot [\![\underline{\xi}]\!](\underline{x}) \\ &\qquad \text{with} \\ &\boldsymbol{K} = K_n \underline{n} \otimes \underline{n} + K_t(\mathbf{1} - \underline{n} \otimes \underline{n}), \quad K_n \to \infty \end{aligned} \tag{9}$$

$\boldsymbol{K}$ is the second-order interface stiffness tensor with infinite normal component $K_n$ (no mutual interpenetration of crystals), and positive tangential component $K_t$ (allowing for relative tangential movements of crystal surfaces). Also the bulk crystal phase inside the RVE $V_{\text{poly}}$ behaves linear elastically,

$$\forall \underline{x} \in V_i : \boldsymbol{\sigma}(\underline{x}) = \mathbb{C}_C : \boldsymbol{\varepsilon}(\underline{x}) \tag{10}$$

with $\mathbb{C}_C = 3k_C\mathbb{J} + 2\mu_C\mathbb{K}$ as the isotropic elastic stiffness of the bulk material phase comprising all single crystals; with bulk modulus $k_C$ and shear modulus $\mu_C$. $\mathbb{J} = 1/3\mathbf{1} \otimes \mathbf{1}$ and $\mathbb{K} = \mathbb{I} - \mathbb{J}$ are the volumetric and the deviatoric part of the fourth-order identity tensor $\mathbb{I}$, with components $I_{ijkl} = 1/2(\delta_{ik}\delta_{jl} + \delta_{il}\delta_{kj})$; the components of the second-order unit tensor $\mathbf{1}$, $\delta_{ij}$ (Kronecker delta), read as $\delta_{ij} = 1$ for $i = j$ and $\delta_{ij} = 0$ for $i \neq j$.

The assumption of crystal isotropy deserves to be commented, since single crystals are generally anisotropic, including approximately transversely isotropic hydroxyapatite [34]. However, hydroxyapatite anisotropy is not very pronounced [34], and in addition, the disorder of crystals (and of their principal material directions) probably renders isotropic phase proporties as suitable approximation for the purpose of polycrystal property homogenization. This was recently shown quantitatively for polycrystals consisting of perfectly disordered needles, being either isotropic or anisotropic [18].

## Homogenized elasticity of polycrystal with compliant interfaces

As long as the interfaces behave elastically, the relation between $\boldsymbol{\Sigma}_{\text{poly}}$ and $\boldsymbol{E}_{\text{poly}}$ reads as

$$\boldsymbol{\Sigma}_{\text{poly}} = \mathbb{C}_{\text{poly}} : \boldsymbol{E}_{\text{poly}} \tag{11}$$

with the 'macroscopic' homogenized stiffness tensor of the polycrystal, $\mathbb{C}_{\text{poly}} = 3k_{\text{poly}}\mathbb{J} + 2\mu_{\text{poly}}\mathbb{K}$, with bulk modulus $k_{\text{poly}}$ and shear modulus $\mu_{\text{poly}}$; depending on the local elastic properties $\mathbb{C}_C$ and $K_t$.

Following [14], the establishment of this dependence is based on the behavior of a composite solid consisting of a spherical inclusion of radius $a$ and a compliant interface coating the inclusion, being itself embedded in an infinite matrix exhibiting the elastic properties $\mathbb{C}_{\text{poly}}$ of the homogenized polycrystal, and being subjected to uniform strains $\boldsymbol{E}_0$ at infinity (Fig. 3).

Mathematically, we have

$$\begin{aligned} r < a \quad &: \quad \boldsymbol{\sigma} = \mathbb{C}_C : \boldsymbol{\varepsilon} \\ r = a \quad &: \quad \underline{T} = \boldsymbol{K}' \cdot [\underline{\xi}] \\ &\quad \text{with } [\underline{\xi}] = [\![\underline{\xi}]\!]/2, \boldsymbol{K}' = 2\boldsymbol{K} \\ r > a \quad &: \quad \boldsymbol{\sigma} = \mathbb{C}_{\text{poly}} : \boldsymbol{\varepsilon} \\ r \to \infty \quad &: \quad \underline{\xi} \to \boldsymbol{E}_0 \cdot \underline{x} \end{aligned} \tag{12}$$

For determination of $k_{\text{poly}}$, a purely spherical deformation, $\boldsymbol{E}_0 = E_0\mathbf{1}$ is imposed at $r \to \infty$. Spherical symmetry of both the loading and the geometry of the considered solid implies vanishing tangential displacement discontinuities at the inclusion interface, $[\![\xi_t]\!] \equiv 0$. Since $K_n \to \infty$, also $[\![\xi_n]\!] = 0$ (no mutual interpenetration of crystals), and the matrix-inclusion problem with compliant interfaces

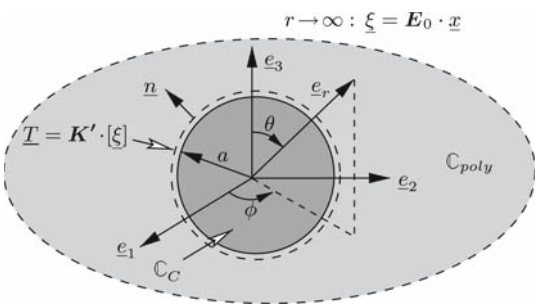


**Fig. 3** Matrix-inclusion problem with compliant interface ('generalized Eshelby problem'): a spherical inclusion with interface is embedded in an infinite matrix subjected to uniform strain $\boldsymbol{E}_0$ at infinity. The elastic properties of the matrix are those of the homogenized material

reduces to the classical Eshelby-type inclusion problem with a perfect, rigid interface [17]. Then, consideration of only one bulk phase (the crystals) implies that the overall bulk modulus $k_{\text{poly}}$ is identical to the crystal bulk modulus $k_C$,

$$k_{\text{poly}} \equiv k_C \tag{13}$$

For determination of $\mu_{\text{poly}}$, a purely deviatoric deformation, $\boldsymbol{E}_0 = E_0(\underline{e}_1 \otimes \underline{e}_1 - \underline{e}_3 \otimes \underline{e}_3)$, is imposed (see Fig. 3 for the Cartesian base frame $\underline{e}_1, \underline{e}_2, \underline{e}_3$). The mathematical form of the displacement field in the exterior region, $r > a$ (the homogenized material), $\underline{\xi}_{\text{ex}}$, is established in the line of [27], and reads in spherical coordinates (see Fig. 3 for Eulerian angles $\phi$ and $\theta$) as

$$\begin{aligned}
\frac{\xi_{\text{ex},r}}{E_0} &= (A_{\text{ex}} r + 3\frac{B_{\text{ex}}}{r^4} + \frac{5-4\nu_{\text{poly}}}{1-2\nu_{\text{poly}}}\frac{C_{\text{ex}}}{r^2})(\cos^2\phi \sin^2\theta - \cos^2\theta) \\
\frac{\xi_{\text{ex},\theta}}{E_0} &= \frac{1}{2}(A_{\text{ex}} r - 2\frac{B_{\text{ex}}}{r^4} + 2\frac{C_{\text{ex}}}{r^2}) \sin 2\theta (1 + \cos^2\phi) \\
\frac{\xi_{\text{ex},\phi}}{E_0} &= -\frac{1}{2}(A_{\text{ex}} r - 2\frac{B_{\text{ex}}}{r^4} + 2\frac{C_{\text{ex}}}{r^2}) \sin\theta \sin 2\phi
\end{aligned} \tag{14}$$

where $\nu_{\text{poly}}$ is the Poisson's ratio of the polycrystal with weak interfaces,

$$\nu_{\text{poly}} = \frac{3k_{\text{poly}} - 2\mu_{\text{poly}}}{6k_{\text{poly}} + 2\mu_{\text{poly}}} \tag{15}$$

The boundary condition in $(12)_4$ directly implies $A_{\text{ex}} = 1$, while the constants $B_{\text{ex}}$ and $C_{\text{ex}}$ will follow from interface conditions.

Inside the inclusion ($r < a$, the solid crystal phase), the displacement field $\underline{\xi}_{\text{in}}$ reads as

$$\begin{aligned}
\frac{\xi_{\text{in},r}}{E_0} &= (A_{\text{in}} r + B_{\text{in}} r^3)(\cos^2\phi \sin^2\theta - \cos^2\theta) \\
\frac{\xi_{\text{in},\theta}}{E_0} &= \frac{1}{2}(A_{\text{in}} r + \frac{(11\mu_C + 15k_C)B_{\text{in}} r^3}{3(3k_C - 2\mu_C)}) \sin 2\theta (1 + \cos^2\phi) \\
\frac{\xi_{\text{in},\phi}}{E_0} &= -\frac{1}{2}(A_{\text{in}} r + \frac{(11\mu_C + 15k_C)B_{\text{in}} r^3}{3(3k_C - 2\mu_C)}) \sin\theta \sin 2\phi
\end{aligned} \tag{16}$$

The four remaining constants $B_{\text{ex}}, C_{\text{ex}}, A_{\text{in}}$ and $B_{\text{in}}$ are determined by enforcing equilibrium of forces at the interface $r = a$:

$$\underline{T} = \boldsymbol{\sigma}_{\text{in}} \cdot \underline{n} = \boldsymbol{\sigma}_{\text{ex}} \cdot \underline{n} = \boldsymbol{K}' \cdot [\underline{\xi}] \tag{17}$$

together with constitutive laws $(12)_1$, $(12)_2$ and $(12)_3$, see Appendix. This solution for the displacement fields $\underline{\xi}_{\text{in}}$ and $\underline{\xi}_{\text{ex}}$ gives access to the traction forces at the interfaces $\underline{T}(r = a) = \boldsymbol{\sigma} \cdot \underline{n}(r = a) = \boldsymbol{K}' \cdot [\underline{\xi}_{\text{ex}}(r = a^+) - \underline{\xi}_{\text{in}}(r = a^-)]$. Their use for estimating the traction forces at the interfaces within the polycrystalline RVE $V_{\text{poly}}$ yields the corresponding 'macroscopic' stress $\boldsymbol{\Sigma}_{\text{poly}}$ according to (6) as

$$\boldsymbol{\Sigma}_{\text{poly}} = \frac{1}{V_C}\int_{\partial V_C} a\underline{n} \otimes (\boldsymbol{\sigma} \cdot \underline{n})(r = a)\mathrm{d}S \tag{18}$$

The solution for the displacements at $r = a^+$ turns out to be, according to $(12)_2$ and (3), $\underline{\xi}(r = a^+) = \underline{\xi}_i + [\![\underline{\xi}]\!]/2$, a suitable estimate for the mean displacement $\bar{\underline{\xi}}$ at the crystal interface $\mathcal{I}_{ij}$. Use of this quantity in (4) yields the corresponding 'macroscopic' strains $\boldsymbol{E}_{\text{poly}}$ in the form

$$\boldsymbol{E}_{\text{poly}} = \frac{1}{V_C}\int_{\partial V_C} \underline{\xi}_{\text{ex}}(a^+) \overset{s}{\otimes} \underline{n}\mathrm{d}S \tag{19}$$

Shear components $\Sigma_{\text{poly},12}$ and $E_{\text{poly},12}$ of 'macroscopic' stresses (18) and strains (19), together with (14)–(17) and (50)–(54), give access to $\mu_{\text{poly}}$, via $\mu_{\text{poly}} = \Sigma_{12}/(2E_{12})$, yielding (after elimination of $E_0$) the following expression,

$$\frac{\mu_C}{\mu_{\text{poly}}} = 1 + 3\left[\frac{5\kappa}{2} + \left(\frac{\mu_C}{8\mu_{\text{poly}}} + \frac{6k_C + 17\mu_C}{57k_C + 4\mu_C}\right)^{-1}\right]^{-1} \tag{20}$$

with the dimensionless quantity $\kappa = K_t' a/\mu_C$. $\kappa \to \infty$ relates to a rigid interface. The higher the rigidity $\kappa$ of the interface, the higher the overall polycrystal shear modulus (Fig. 4), for different (dimensionless) compressibilities $\chi = \mu_C/k_C$ of the single crystals. Thereby, crystal incompressibility ($\chi \to 0$) guarantees finite overall shear stiffness even for an interface with vanishing stiffness ($\kappa = 0$), while a polycrystal built up of crystals with zero bulk modulus ($\chi \to \infty$) and connected through zero-stiffness interfaces ($\kappa = 0$) does not exhibit

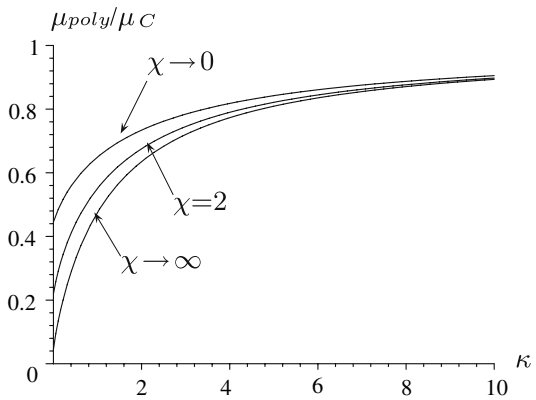


**Fig. 4** Homogenized shear modulus $\mu_{\text{poly}}$ of polycrystal, as function of dimensionless quantity $\kappa = K_t' a/\mu_C$ (interfacial rigidity), for different crystal compressibilities $\chi = \mu_C/k_C$, Eq. 20

any shear stiffness (Fig. 4), but still the bulk stiffness of the single crystals according to (13). In case of an incompressible solid ($k_C \to \infty, \chi = \mu_C/k_C \to 0$), it follows from (13) that $k_{\text{poly}} \to \infty$, and (20) reduces to

$$48(5+\kappa)\left(\frac{\mu_{\text{poly}}}{\mu_C}\right)^2 + (-114+9\kappa)\frac{\mu_{\text{poly}}}{\mu_C} - 57\kappa = 0 \qquad (21)$$

## Upscaled failure properties of polycrystal with weak interfaces

In order to determine the effective failure properties resulting from local failure characteristics (8) and from the interactions between interfaces and bulk single crystals, we are left with relating the local interface forces $\underline{T}(\underline{x}) \in \mathcal{I}$ to the 'macroscopic' stresses $\boldsymbol{\Sigma}_{\text{poly}}$, see (5). The tangential and normal traction forces, $T_t$ and $T_n$, occuring in the interface failure criterion (8), are non-homogeneously distributed across the interfaces. Failure will occur where relatively high tangential traction forces encounter a relative low resistance due to relatively low normal traction forces. Instead of trying to model the actual force fields across the interfaces, we estimate the effect of the actual force distribution through so-called *effective* traction forces, as it is commonly done for stress, strain, or force fields in the context of continuum micromechanics [14, 47]. In this line, we represent the failure-inducing interplay between moderate normal traction forces and tangential traction force *peaks* by means of two different *effective* measures for the normal and the tangential traction forces, respectively: (i) first-order moments of normal forces, and (ii) second-order moments of tangential forces.

The first-order moment of the normal traction forces, $\langle T_n \rangle$, is related to the 'macroscopic' mean stress $\Sigma_{\text{poly},m}$ through

$$\begin{aligned}\Sigma_{\text{poly},m} &= \frac{1}{3}\text{tr}\boldsymbol{\Sigma}_{\text{poly}} \\ &= \frac{1}{3}\text{tr}\left(\frac{3}{A_C}\int_{\partial V_C} \underline{n}(\underline{x}) \otimes [\boldsymbol{\sigma}(\underline{x})\cdot\underline{n}(\underline{x})]\text{d}S\right) \\ &= \frac{1}{A_C}\int_{\partial V_C} \sigma_{rr}(\underline{x})\text{d}S = \frac{1}{A_C}\int_{\partial V_C} T_n(\underline{x})\text{d}S \\ &= \langle T_n \rangle \end{aligned} \qquad (22)$$

(22) establishes a first link between the 'macroscopic' stress $\boldsymbol{\Sigma}_{\text{poly}}$ and the interface tractions $\underline{T}(\underline{x})$: We use this average (or first-order moment) of normal traction forces as to estimate the 'average' interface resistance $T_t^{\text{cr}}$ in (8), according to

$$T_t^{\text{cr}} \approx \alpha(h - \langle T_n \rangle) \qquad (23)$$

However, use of the average tangential traction force $\langle T_t \rangle$ in failure criterion (8) is problematic since force peaks initializing failure may be cancelled out in the averaging process. As a remedy, we use the second-order moment $\sqrt{\langle T_t^2 \rangle}$ (also called quadratic average) as a characteristic or *effective* value for $T_t(\underline{x})$, in the line of [13, 14, 35]. The relation between $\sqrt{\langle T_t^2 \rangle}$ and $\boldsymbol{\Sigma}_{\text{poly}}$ is established through energy considerations: The energy stored in the RVE $V_{\text{poly}}$ can be expressed through the global 'macroscopic' energy density $\Psi$ as

$$\begin{aligned} V_{\text{poly}}\Psi &= \frac{1}{2}V_{\text{poly}}\boldsymbol{\Sigma}_{\text{poly}} : \boldsymbol{E}_{\text{poly}} \\ &= \frac{1}{2}V_{\text{poly}}\boldsymbol{E}_{\text{poly}} : \mathbb{C}_{\text{poly}} : \boldsymbol{E}_{\text{poly}} \\ &= V_{\text{poly}}\left(\frac{1}{2}k_{\text{poly}}E_{\text{poly,v}}^2 + 2\mu_{\text{poly}}E_{\text{poly,d}}^2\right) \end{aligned} \qquad (24)$$

with 'macroscopic' volumetric strain $E_{\text{poly,v}} = \text{tr}\boldsymbol{E}_{\text{poly}}$ and equivalent deviatoric strain $E_{\text{poly,d}} = \sqrt{1/2\boldsymbol{E}_{\text{poly,d}} : \boldsymbol{E}_{\text{poly,d}}}, \boldsymbol{E}_{\text{poly,d}} = \boldsymbol{E}_{\text{poly}} - 1/3E_{\text{poly,v}}\mathbf{1}$.

In order to express $\Psi$ from a microstructural viewpoint, we consider the local constitutive behavior of the interface (Eq. 9) and of the bulk phase (Eq. 10). The corresponding 'macroscopic' elastic energy stored in the RVE reads as

$$\begin{aligned} V_{\text{poly}}\Psi &= \frac{1}{2}\int_{V_{\text{poly}}} \boldsymbol{\sigma} : \boldsymbol{\varepsilon}\text{d}V + \frac{1}{2}\int_{\mathcal{I}} \underline{T}\cdot[\![\underline{\xi}]\!]\text{d}S \\ &= \frac{1}{2}\int_{V_{\text{poly}}} \boldsymbol{\varepsilon} : \mathbb{C}_C : \boldsymbol{\varepsilon}\text{d}V + \frac{1}{2}\int_{\mathcal{I}} [\![\underline{\xi}]\!]\cdot\boldsymbol{K}\cdot[\![\underline{\xi}]\!]\text{d}S \end{aligned} \qquad (25)$$

In order to extract $\langle T_t^2 \rangle = \frac{1}{A_C}\int_{\mathcal{I}} T_t^2\text{d}S$ from (25), variations of $\Psi$ with varying $K_t$ (holding merely $\boldsymbol{E}_{\text{poly}}$ fixed) are studied,

$$\begin{aligned} V_{\text{poly}}\frac{\partial\Psi}{\partial K_t} &= \int_{V_{\text{poly}}} \frac{\partial\boldsymbol{\varepsilon}}{\partial K_t} : \boldsymbol{\sigma}\text{d}V + \int_{\mathcal{I}} \frac{\partial[\![\underline{\xi}]\!]}{\partial K_t}\cdot\underline{T}\text{d}S \\ &\quad + \frac{1}{2}\int_{\mathcal{I}} [\![\underline{\xi}]\!]\cdot(\mathbf{1}-\underline{n}\otimes\underline{n})\cdot[\![\underline{\xi}]\!]\text{d}S = \int_{V_{\text{poly}}} \frac{\partial\boldsymbol{\varepsilon}}{\partial K_t} : \boldsymbol{\sigma}\text{d}V \\ &\quad + \int_{V_{\text{poly}}} \frac{\partial}{\partial K_t}([\![\underline{\xi}]\!]\otimes\underline{n}\delta_{\mathcal{I}}) : \boldsymbol{\sigma}\text{d}V + \frac{1}{2}\int_{\mathcal{I}} [\![\xi_t]\!]^2\text{d}S \end{aligned} \qquad (26)$$

where $\underline{T} = \boldsymbol{\sigma}\cdot\underline{n}$ was considered and where $\delta_{\mathcal{I}}$ is the 'Dirac distribution' of support $\mathcal{I}$, $\int_V \delta_{\mathcal{I}} f\text{d}V = \int_{\mathcal{I}} f\text{d}S$. For transformation of (26), we extend Hill's lemma [28] to the case of displacement discontinuities at the interfaces [14]. Considering (5) and the format (2) for the 'macroscopic' strains $\boldsymbol{E}_{\text{poly}}$, (26) can be transformed to

$$\begin{aligned} V_{\text{poly}}\frac{\partial\Psi}{\partial K_t} &= \int_{V_{\text{poly}}} \frac{\partial}{\partial K_t}(\boldsymbol{\varepsilon} + [\![\underline{\xi}]\!]\otimes\underline{n}\delta_{\mathcal{I}}) : \boldsymbol{\sigma}\text{d}V \\ &\quad + \frac{1}{2}\int_{\mathcal{I}} [\![\xi_t]\!]^2\text{d}S = \frac{\partial\boldsymbol{E}_{\text{poly}}}{\partial K_t} : \boldsymbol{\Sigma}_{\text{poly}} + \frac{1}{2}\int_{\mathcal{I}} [\![\xi_t]\!]^2\text{d}S \end{aligned} \qquad (27)$$

*Fixed* 'macroscopic' strains $\boldsymbol{E}_{\text{poly}}$ according to (1) imply $\partial \boldsymbol{E}_{\text{poly}}/\partial K_t = \boldsymbol{0}$, so that (27) becomes

$$V_{\text{poly}} \frac{\partial \Psi}{\partial K_t} = \frac{1}{2} \int_{\mathcal{I}} [\![\xi_t]\!]^2 \mathrm{d}S = \frac{\mathcal{I}}{2} \left\langle [\![\xi_t]\!]^2 \right\rangle \tag{28}$$

Identification of (28) with the derivation of the 'macroscopic' expression for the energy density (24) with respect to $K_t$ yields

$$\frac{\mathcal{I}}{V_{\text{poly}}} \left\langle [\![\xi_t]\!]^2 \right\rangle = \frac{\partial k_{\text{poly}}}{\partial K_t} E^2_{\text{poly},v} + 4 \frac{\partial \mu_{\text{poly}}}{\partial K_t} E^2_{\text{poly},d} \tag{29}$$

When considering $\langle T_t^2 \rangle = K_t^2 \langle [\![\xi_t^2]\!] \rangle$ according to (9), $\partial k_{\text{poly}}/\partial K_t = 0$ according to (13), and $\Sigma_{\text{poly},d} = 2\mu_{\text{poly}} E_{\text{poly},d}$, (29) reduces to

$$\frac{\mathcal{I}}{V_{\text{poly}}} \langle T_t^2 \rangle = -\frac{\partial}{\partial K_t} \left( \frac{1}{\mu_{\text{poly}}} \right) K_t^2 \Sigma^2_{\text{poly},d} \tag{30}$$

where $\Sigma_{\text{poly},d}$ is the equivalent deviatoric stress of the 'macroscopic' second-order stress tensor $\boldsymbol{\Sigma}_{\text{poly}}$,

$$\begin{aligned} \Sigma_{\text{poly},d} &= \sqrt{\frac{1}{2} \boldsymbol{\Sigma}_{\text{poly},d} : \boldsymbol{\Sigma}_{\text{poly},d}} \\ \text{with } \boldsymbol{\Sigma}_{\text{poly},d} &= \boldsymbol{\Sigma}_{\text{poly}} - \Sigma_{\text{poly},m} \boldsymbol{1}, \\ \text{and } \Sigma_{\text{poly},m} &= \frac{1}{3} \text{tr} \boldsymbol{\Sigma}_{\text{poly}} \end{aligned} \tag{31}$$

Combination of (30) with $\mathcal{I}/V_{\text{poly}} = 3/(2a)$ and with $\kappa = K_t' a/\mu_C$ yields

$$\begin{aligned} \sqrt{\langle T_t^2 \rangle} &= \mathcal{B}_{T_t} \Sigma_{\text{poly},d} \\ \text{with } \mathcal{B}_{T_t}(\chi = \frac{\mu_C}{k_C}, \kappa) &= \sqrt{-\frac{1}{3} \kappa^2 \frac{\partial}{\partial \kappa} \left( \frac{\mu_C}{\mu_{\text{poly}}} \right)} \end{aligned} \tag{32}$$

Remarkably, the second-order moment of tangential tractions over all interfaces within the RVE, $\sqrt{\langle T_t^2 \rangle}$, is proportional to the 'macroscopic' equivalent deviatoric stress $\Sigma_{\text{poly},d}$, expressed by the proportionality factor $\mathcal{B}_{T_t}$. The more compressible the solid crystal (the larger $\chi = \mu_C/k_C$), the higher the tangential traction peaks in the intercrystalline interface, generated by an equivalent deviatoric 'macroscopic' stress $\Sigma_{\text{poly},d}$. However, the corresponding concentration factor $\mathcal{B}_{T_t}$ is bounded by $\sqrt{2/5}$ (Fig. 5),

$$\lim_{\chi \to \infty} \mathcal{B}_{T_t}(\kappa) = \sqrt{\frac{2}{5}} \tag{33}$$

On the other hand, for any constant crystal compressibility $\chi$, stiffening the interface (enlarging $\kappa = K_t' a/\mu_C$) also increases the peaks of tangential traction force, i.e., the proportionality factor $\mathcal{B}_{T_t}$, again bounded by $\sqrt{2/5}$ (Fig. 5),

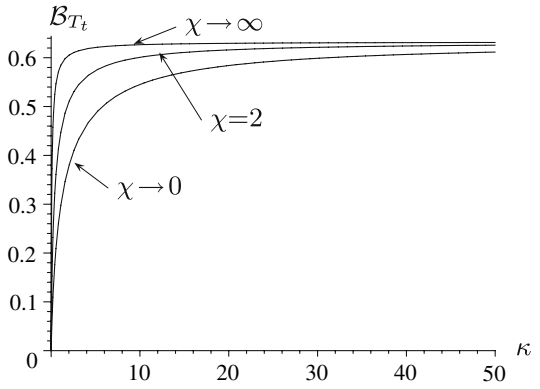


**Fig. 5** Concentration factor $\mathcal{B}_{T_t}$ relating 'macroscopic' deviatoric stress on polycrystal to effective tangential traction in intercrystalline interfaces, as function of dimensionless quantity $\kappa = K_t' a/\mu_C$ (interfacial rigidity), for different crystal compressibilities $\chi = \mu_C/k_C$, Eq. 32

$$\lim_{\kappa \to \infty} \mathcal{B}_{T_t}(\chi) = \sqrt{\frac{2}{5}} \tag{34}$$

Use of the micro traction-macro stress relationships (22) and (32) in the local interface criterion (8) yields a 'macroscopic' polycrystal-specific brittle-failure criterion in the form

$$\mathcal{B}_{T_t} \Sigma_{\text{poly},d} \leq \alpha (h - \Sigma_{\text{poly},m}) \tag{35}$$

(35) expresses that Coulomb-type brittle failure (8) in the interfaces between spherical crystals inside the RVE results in Drucker–Prager-type (brittle) failure properties at the scale of the polycrystal.

## Micromechanics of porous material with polycrystalline skeleton

We consider an RVE $V_{\text{PORO}}$ (Figs. 2b, 9) of a porous material (with porosity $\varphi$) where the contiguous solid phase [volume $V_S$, $V_S = V_{\text{PORO}}(1-\varphi)$] is a polycrystal with weak interfaces according to Section "Micromechanics of polycrystal with weak interfaces". The Mori–Tanaka homogenization scheme has been proven as suitable tool to upscale the elastic properties of the solid phase [$k_{\text{poly}}$ and $\mu_{\text{poly}}$ defined through (13), (20), (21)] to the stiffness of such a porous material, see e.g. [9, 11],

$$\mathbb{C}_{\text{PORO}} = (1-\varphi)\mathbb{C}_{\text{poly}} : \left( (1-\varphi)\mathbb{I} + \varphi(\mathbb{I} - \mathbb{S})^{-1} \right)^{-1} \tag{36}$$

with the Eshelby tensor $\mathbb{S}$ for spherical inclusions reading as [17]

$$\mathbb{S} = \frac{3k_{\text{poly}}}{3k_{\text{poly}} + 4\mu_{\text{poly}}}\mathbb{J} + \frac{6(k_{\text{poly}} + 2\mu_{\text{poly}})}{5(3k_{\text{poly}} + 4\mu_{\text{poly}})}\mathbb{K} \tag{37}$$

so that

$$k_{\text{PORO}} = \frac{4k_{\text{poly}}\mu_{\text{poly}}(1-\varphi)}{3k_{\text{poly}}\varphi + 4\mu_{\text{poly}}} \tag{38}$$

$$\mu_{\text{PORO}} = \mu_{\text{poly}}\frac{(1-\varphi)(9k_{\text{poly}} + 8\mu_{\text{poly}})}{9k_{\text{poly}}(1+\frac{2}{3}\varphi) + 8\mu_{\text{poly}}(1+\frac{3}{2}\varphi)} \tag{39}$$

We consider brittle failure of the overall porous medium if the polycrystal failure criterion (35) is reached in highly stressed regions of the polycrystalline matrix. The corresponding ('micro'-) heterogeneity within the solid matrix has recently been shown [13] to be reasonably considerable through so-called (homogeneous) *effective* ('micro'-) stresses, such as the square root of the spatial average over the solid material phase, of the squares of equivalent deviatoric ('micro'-) stresses,

$$\sqrt{\langle\sigma_d^2\rangle_S} = \sqrt{\frac{1}{V_S}\int_{V_S}\frac{1}{2}\boldsymbol{\sigma}_d(\underline{x}) : \boldsymbol{\sigma}_d(\underline{x})\mathrm{d}V} \tag{40}$$

$$\text{with } \boldsymbol{\sigma}_d(\underline{x}) = \boldsymbol{\sigma}(\underline{x}) - \frac{1}{3}\text{tr}\boldsymbol{\sigma}(\underline{x})\mathbf{1} \tag{41}$$

The effective deviatoric stress (40), used to approximate $\Sigma_{\text{poly},d}$ in (35), is accessible through energy considerations similar to those of (24) to (30), and result to be ([9, p. 132, 13])

$$\Sigma_{\text{poly},d}^2 \approx \langle\sigma_d^2\rangle_S = \left[-\frac{\partial}{\partial\mu_{\text{poly}}}\left(\frac{1}{k_{\text{PORO}}}\right)\Sigma_{\text{PORO},m}^2 - \frac{\partial}{\partial\mu_{\text{poly}}}\left(\frac{1}{\mu_{\text{PORO}}}\right)\Sigma_{\text{PORO},d}^2\right]\frac{\mu_{\text{poly}}^2}{(1-\varphi)} \tag{42}$$

In analogy to (23), the effective mean stress level in the solid matrix is chosen as the stress average over the solid phase,

$$\Sigma_{\text{poly},m} \approx \langle\sigma_m\rangle_S = \frac{1}{V_S}\int_{V_S}\frac{1}{3}\text{tr}\boldsymbol{\sigma}(\underline{x})\mathrm{d}V = \frac{\Sigma_{\text{PORO},m}}{1-\varphi} \tag{43}$$

Use of Eqs. 43 and 42, together with (38)–(41), (13), and (20), in (35) yields a failure criterion at the scale of the porous material with polycrystalline interfaces in the solid phase,

$$\left[\frac{3\varphi}{4} - \left(\frac{\alpha}{\mathcal{B}_{T_t}}\right)^2\right]\Sigma_{\text{PORO},m}^2 + \left[\frac{2\varphi(23 - 50\nu_{\text{poly}} + 35\nu_{\text{poly}}^2)}{(-7+5\nu_{\text{poly}})^2} + 1\right]\Sigma_{\text{PORO},d}^2 + 2\left(\frac{\alpha}{\mathcal{B}_{T_t}}\right)^2 h(1-\varphi)\Sigma_{\text{PORO},m} = \left(\frac{\alpha}{\mathcal{B}_{T_t}}\right)^2 h^2(1-\varphi)^2 \tag{44}$$

with $\nu_{\text{poly}} = \nu_{\text{poly}}(k_{\text{poly}}, \mu_{\text{poly}})$ according to (15), $\mu_{\text{poly}} = \mu_{\text{poly}}(k_C, \mu_C, \kappa)$ according to (20), and $\mathcal{B}_{T_t} = \mathcal{B}_{T_t}(\chi = \frac{\mu_C}{k_C}, \kappa)$ according to (32).

The elastic stress domain of the porous medium the matrix of which is a polycrystal with brittle interfaces increases with decreasing crystal compressibility $\chi$ (Fig. 6). For the incompressible limit case, $\chi \to 0$, (44) reduces to

$$\left[\frac{3\varphi}{4} - \left(\frac{\alpha}{\mathcal{B}_{T_t}}\right)^2\right]\Sigma_{\text{PORO},m}^2 + \left(1+\frac{2}{3}\varphi\right)\Sigma_{\text{PORO},d}^2 + 2\left(\frac{\alpha}{\mathcal{B}_{T_t}}\right)^2 h(1-\varphi)\Sigma_{\text{PORO},m} = \left(\frac{\alpha}{\mathcal{B}_{T_t}}\right)^2 h^2(1-\varphi)^2 \tag{45}$$

For a crystal compressibility of hydroxyapatite, $\chi \approx 0.54$ (see also Section "Application to hydroxyapatite biomaterials"), the elastic domain increases with decreasing interfacial rigidity (Fig. 7) and with increasing friction angle $\alpha$ (Fig. 8). High interfacial rigidities $\kappa$ or low friction angles $\alpha$ result in closed elastic domains, indicating possible failure of the porous material even under hydrostatic stress states $\boldsymbol{\Sigma} = \mathbf{1}\Sigma_m$, while low interfacial rigidities $\kappa$ or high friction angles $\alpha$ are related to open elastic domains, related to infinite resistance of the porous material, as long

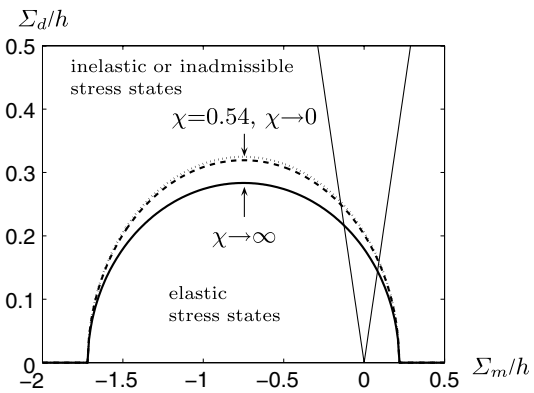


**Fig. 6** Elastic limits of a porous material the matrix of which is a polycrystal with brittle interfaces, for different crystal compressibilities $\chi = \mu_C/k_C$ (Eq. 44): $\varphi = 0.5, \alpha = 0.3, \kappa \to \infty$. Uniaxial load path indicated (thin solid line)

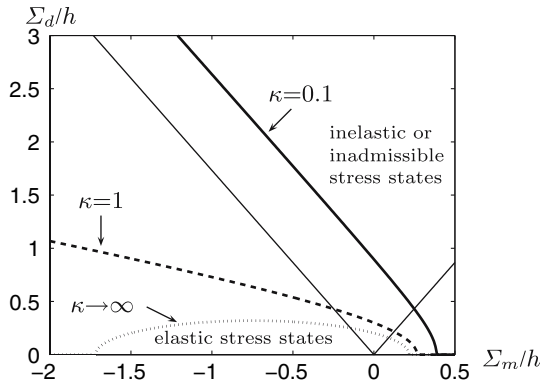


**Fig. 7** Elastic limits of a porous material the matrix of which is a polycrystal with brittle interfaces, for different dimensionless quantities $\kappa = K_t' a/\mu_C$ (interfacial rigidity) (Eq. 44): $\varphi = 0.5$, $\alpha = 0.3, \chi = 0.54$. Uniaxial load path indicated (thin solid line)

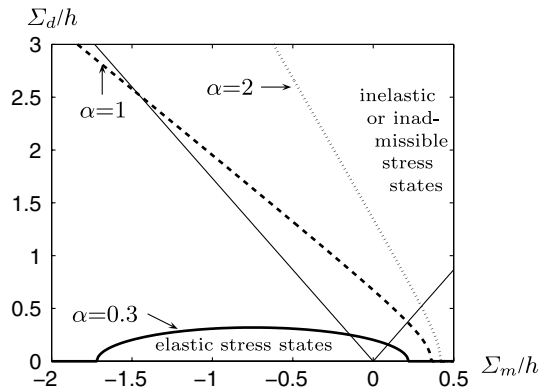


**Fig. 8** Elastic limits of a porous material the matrix of which is a polycrystal with brittle interfaces, for different friction angles $\alpha$ (Eq. 44): $\varphi = 0.5, \kappa \to \infty, \chi = 0.54$. Uniaxial load path indicated (thin solid line)

as the macroscopic stress state $\boldsymbol{\Sigma}$ contains a certain hydrostatic amount (Figs. 7 and 8).

## Application to hydroxyapatite biomaterials

Porous hydroxyapatite (HA) biomaterials are widely used for replacement of hard tissue defects, because of their chemical composition, microstructure and Young's modulus being similar to the bone mineral, called carbonated or calcium-deficient hydroxyapatite (CDHA) [26, 36, 46]. If porous scaffolds are used as bone replacement material in highly loaded anatomical locations, reliability of their mechanical properties is particularly important for the performance of the implants. Therefore, the prediction of strength of HA biomaterials from their microstructure and porosity is of particular interest. To the knowledge of the authors, corresponding micromechanical approaches are extremely rare or inexistent, so that we check in this section, to which extent the model developed before can serve the purpose of the aforementioned prediction.

**Table 2** Experimental data: Compressive strength $f_c$ as function of porosity $\varphi$, for artificial hydroxyapatite produced through different synthesis routes

| Peelen et al. [42] | | Akao et al. [1] | | Martin and Brown [38] | |
|---|---|---|---|---|---|
| $\varphi$ (%) | $f_c$ (MPa) | $\varphi$ (%) | $f_c$ (MPa) | $\varphi$ (%) | $f_c$ (MPa) |
| 36 | 160 | 2.8 | 509 | 27 | 172.5[a] |
| 48 | 114 | 3.9 | 465 | 39 | 119[a] |
| 60 | 69 | 9.1 | 415 | | |
| 65 | 45 | 19.4 | 308 | | |
| 70 | 30 | | | | |

[a] Mean value calculated from three experiments

### Materials processing and uniaxial mechanical testing

We here consider the following artificially produced HA materials: Peelen et al. [42] controlled the porosity of HA by a variation of the sintering temperature (1,100–1,400 °C, Table 2). Compacted commercially available powders were used to produce HA with porosities between 36% and 70%. Cylindrical samples (diameter: 1 cm, length: 1–1.5 cm) were tested in compression (Table 2).

Akao et al. [1] precipitated HA powder and sintered it at different temperatures (1,150–1,300 °C). Porosities ranged from 3% to 19% (Table 2). Compression tests were performed on bars with dimensions of $5 \times 5 \times 10$ cm$^3$ (Table 2).

Martin and Brown [38] prepared calcium-deficient HA formed in aqueous solutions at physiological temperatures. The authors realized two different liquid-to-solid weight ratios, resulting in porosities of 27% and 39%, respectively (Table 2). Cylindrical samples with diameter of ~6 mm were tested in compression (Table 2).

### Micromechanical representation of hydroxyapatite biomaterials

In the hierarchical organization of synthetic hydroxyapatite ceramics, we identify two different scales which will be considered in the framework of a two-step homogenization scheme. The first homogenization step refers to an observation scale of several hundreds of microns where hydroxyapatite crystals are separated by boundaries or interfaces (Fig. 9a). The latter will be shown to be a potential nucleus for failure of the material. The corresponding homogenized material is called 'hydroxyapatite polycrystal with interfaces'. At the microstructural scale with a characteristic length of some millimeters (Fig. 9b), pores are embedded in a matrix which is made up of the material which was homogenized in the first upscaling step.

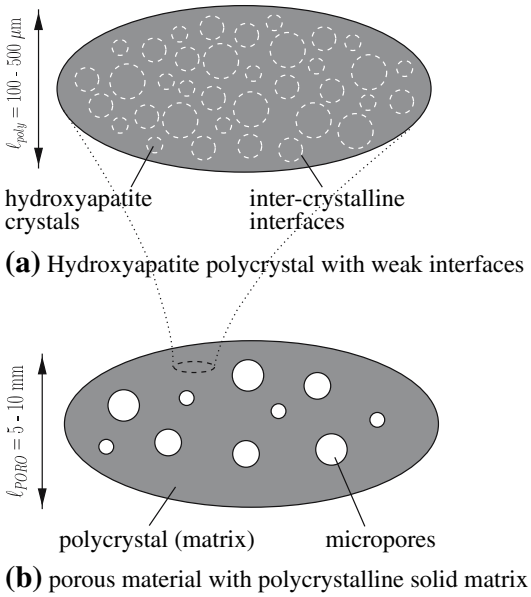


**(a)** Hydroxyapatite polycrystal with weak interfaces

**(b)** porous material with polycrystalline solid matrix

**Fig. 9** Micromechanical representation of a porous hydroxyapatite polycrystal by means of a two-step homogenization procedure. (**a**) Hydroxyapatite polycrystal with weak interfaces and (**b**) porus material with polycrystalline solid matrix

Elastic properties of single crystals of hydroxyapatite

An ultrasonic interferometer technique delivers typical values for bulk and shear moduli, $k_C = k_{HA} = 82.6\,\text{GPa}$ and $\mu_C = \mu_{HA} = 44.9\,\text{GPa}$ [34].

Biomaterial-independent properties of interfaces between hydroxyapatite crystals, $\alpha, h, \kappa$—back-analysis

The expression for macroscopic admissible stress states (44) contains three material properties which are difficult to be directly accessed, namely the friction angle $\alpha$, the cohesion $h$, and the rigidity $\kappa$ of the interfaces. Therefore, these phase properties will be determined by means of an optimization procedure providing the closest match of model predictions to experimentally determined uniaxial compressive strength data of hydroxyapatite biomaterials, given in Table 2 [1, 38, 42].

The sum of squares of relative errors between predicted strength and experimental strength values is minimized,

$$\mathcal{G}(\alpha,h,\kappa) = \sum_i \left( \frac{f_{c,i}^{\text{pred}} - f_{c,i}^{\text{exp}}}{f_{c,i}^{\text{exp}}} \right)^2 \to 0 \quad \Rightarrow \alpha^{\text{opt}}, h^{\text{opt}}, \kappa^{\text{opt}} \tag{46}$$

where $f_{c,i}^{\text{pred}}$ denotes predicted uniaxial compressive strength values obtained from Eq. 44 with $\Sigma_{\text{PORO},m} = -f_{c,i}^{\text{pred}}/3$, $\Sigma_{\text{PORO},d} = f_{c,i}^{\text{pred}}/\sqrt{3}$, together with Eqs. 13, 20, and 32, for porosity values $\varphi_i$ according to Table 2. $f_{c,i}^{\text{exp}}$ is the corresponding $i$th experimental strength value, see Table 2.

We use the 'two-membered evolution strategy' [24, 45], closely related to the ideas of Darwin's evolution theory. The components of a three-dimensional vector of estimations for $\alpha$, $h$ and $\kappa$, $(\alpha,h,\kappa)_{\text{parent}}$, representing the 'parent', are slightly varied by help of a random number generator (representing 'mutations'), resulting in a vector $(\alpha,h,\kappa)_{\text{child}}$, representing the 'child',

$$(\alpha,h,\kappa)_{\text{child}} = (\alpha,h,\kappa)_{\text{parent}} + (\mathcal{N}\sigma\alpha_{\text{parent}}, \mathcal{N}\sigma h_{\text{parent}}, \mathcal{N}\sigma\kappa_{\text{parent}}) \tag{47}$$

$\mathcal{N}$ denotes a number produced by a standardized normally distributed random number generator standardly available in MATLAB [31]. $\sigma$ stands for a scattering factor which will be dealt with later on.

If the child fits better in its 'environment' than the parent, i.e., if

$$\mathcal{G}[(\alpha,h,\kappa)_{\text{child}}] < \mathcal{G}[(\alpha,h,\kappa)_{\text{parent}}] \tag{48}$$

see (46), vector $(\alpha,h,\kappa)_{\text{child}}$ will be further varied, i.e., it then becomes the parent for the next generation. If not, the original parent undergoes new mutations.

Based on the number of 'successes' of the evolution, i.e., the number of cases for which Eq. 48 holds, the scattering factor $\sigma$ is changed: If the total number of successes within the last 10 mutations exceeds a certain threshold (typically 4), $\sigma$ is enlarged, otherwise it is reduced.

If the difference between $\mathcal{G}[(\alpha,h,\kappa)_{\text{parent}}]$ and $\mathcal{G}[(\alpha,h,\kappa)_{\text{child}}]$ lies within a prescribed tolerance over a certain number of mutations, the optimum $(\alpha^{\text{opt}}, h^{\text{opt}}, \kappa^{\text{opt}}) \approx (\alpha,h,\kappa)_{\text{parent}} \approx (\alpha,h,\kappa)_{\text{child}}$ has been reached.

Applying this procedure, (46)–(48), to (44) and using the experimental data from Table 2 yields, depending on the start values of the optimization procedure, a set of solution vectors $(\alpha^{\text{opt}}, h^{\text{opt}}, \kappa^{\text{opt}})$ which are equal in terms of the highly satisfactory correlation coefficient $(r^2 = 0.97)$ between the respective model predictions and the corresponding experimental data for uniaxial compressive strength (see Fig. 10). To give an example, $(\alpha^{\text{opt}}, h^{\text{opt}}, \kappa^{\text{opt}}) = (0.6750, 17.2397, 0.9119)$ and (0.9345, 17.7664, 6.4160) ($h$ has the dimension (MPa)) are two of these solution vectors. For all calculated 'optimal' solution vectors, we find a constant ratio $\alpha' = \alpha/\mathcal{B}_{T_i} = 1.61$ (see Eqs. 20 and 32), implying a relationship between $\alpha$ and $\kappa$, depicted in Fig. 11.

Clearly, it would be interesting to cross-check these interface failure parameters derived from our 'inverse method' with other direct tests. Deplorably, an extensive literature check could not provide any direct in situ measurements of stresses and failure mechanisms at the interface 'micro' level. The only additional experimental

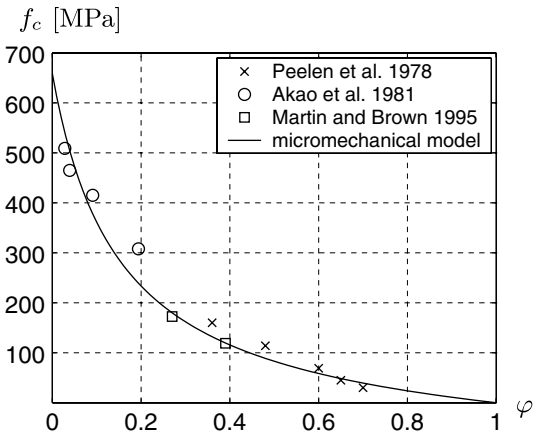


**Fig. 10** Uniaxial compressive strength $f_c$ of porous hydroxyapatite biomaterial as function of porosity $\varphi$: model prediction according to Eq. 44 or Eq. 49, evaluated with $\Sigma_{\text{PORO},m} = -f_c/3, \Sigma_{\text{PORO},d} = f_c/\sqrt{3}$, compared to experimental data (Table 2). Correlation coefficient $r^2 = 0.97$

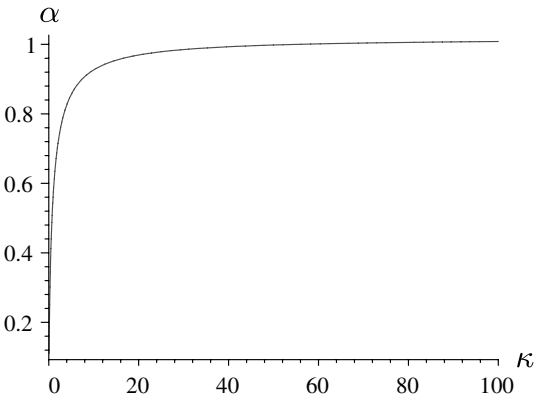


**Fig. 11** Friction angle–interface rigidity relationship $\alpha(\kappa)$ suitable for representation of strength of hydroxyapatite biomaterials (Fig. 10)

evidence are scanning electron micrographs (Fig. 2 in Ref. [8], Figs. 5–7 in Ref. [38]): These images, however, clearly show sharp, rough failure surfaces, coinciding with the boundaries of single, micrometer-sized grains. This, together with the sharp stress drops in corresponding ('macroscopic') stress–strain diagrams indicating brittle overall failure, strongly suggests brittle failure of the crystal interfaces, as we have modeled herein.

### Brittle versus ductile failure of solid matrix in porous medium

From a purely mathematical standpoint, it is interesting to compare the elastic domain (44) to the yield surface of a porous medium, related to failure of a ductile (not a brittle) solid matrix obeying Drucker–Prager criterion (35). This yield surface can be obtained through non-linear homogenization based on effective quantities (42) and (43), as detailed in [9, 11],

$$\left(\frac{3\varphi}{4} - \alpha'^2\right)\Sigma^2_{\text{PORO},m} + \left(1 + \frac{2}{3}\varphi\right)\Sigma^2_{\text{PORO},d} + 2\alpha'^2 h(1-\varphi)\Sigma_{\text{PORO},m} = \alpha'^2 h^2 (1-\varphi)^2 \tag{49}$$

with $\alpha' = \alpha/\mathcal{B}_{T_t}(\kappa)$ and $h$ as only two parameters being left for an optimization procedure to match the experimental data of Fig. 10 and Table 2. This procedure delivers a cohesion $h^{\text{opt}} = 16.51$ MPa (close to the values obtained for the brittle case in Section "Biomaterial-independent properties of interfaces between hydroxyapatite crystals, $\alpha, h, \kappa$—back-analysis") and ratio $\alpha'^{opt} = 1.61$ which is quasi-identical to the one obtained for the brittle case (Section "Biomaterial-independent properties of interfaces between hydroxyapatite crystals, $\alpha, h, \kappa$—back-analysis"), implying an $\alpha$–$\kappa$-relationship quasi-identical to that of Fig. 11. This means that the failure of porous hydroxyapatite biomaterials can be equally well represented by a brittle elastic-limit-type micromechanics model and a ductile one related to limit analysis. In this context, it is very interesting to note that the *ductile* criterion (49) is even *identical* to the elastic domain for *incompressible* solid matrices, Eq. 45.

Accordingly, one might argue that the nature of the heterogeneity of the stresses in the solid matrix (considered herein by quadratic averages) is far more important for the overall failure of the material than the precise mode of local interface failure (brittle or ductile). However, as regards hydroxyapatite biomaterials, experiments [7, 38, 43] strongly support brittle failure: A comprehensive mechanical formulation for its possible origin, namely breaking of weak interfaces between hydroxyapatite crystals, was the main focus of the present paper.

## Appendix

### Solution of matrix-inclusion problem with compliant interface ('generalized Eshelby problem', Fig. 3)

Solution of Eqs. 12–14, and 16 for the constants $B_{\text{ex}}, C_{\text{ex}}, A_{\text{in}}$, and $B_{\text{in}}$ yields them as:

$$\begin{aligned} B_{\text{ex}} = -a^5 (&176\mu^3_{\text{poly}}\mu^2_C + 24\mu^2_{\text{poly}}\mu^3_C \\ &- 12\mu^3_C a k_{\text{poly}} K_t - 171\mu^2_C a k_{\text{poly}} K_t k_C + 240\mu^3_{\text{poly}} k_C \mu_C \\ &+ 136\mu^3_{\text{poly}}\mu_C a K_t + 48\mu^3_{\text{poly}} a K_t k_C - 132 a \mu^2_{\text{poly}} K_t \mu^2_C \\ &+ 528\mu^2_{\text{poly}} k_{\text{poly}} \mu^2_C + 9a\mu^2_{\text{poly}} K_t k_C \mu_C \\ &+ 720\mu^2_{\text{poly}} k_{\text{poly}} k_C \mu_C + 342\mu^2_{\text{poly}}\mu^2_C k_C \\ &+ 144\mu^2_{\text{poly}} a k_{\text{poly}} K_t k_C + 408\mu^2_{\text{poly}} a k_{\text{poly}} K_t \mu_C \\ &+ 27 a K_t k_C k_{\text{poly}} \mu_{\text{poly}} \mu_C - 396 a K_t \mu^2_C k_{\text{poly}} \mu_{\text{poly}} \\ &- 57\mu_{\text{poly}}\mu^2_C a K_t k_C - 4\mu_{\text{poly}}\mu^3_C a K_t)/\mathcal{N} \end{aligned} \tag{50}$$

$$C_{\text{ex}} = 5a^3(48\mu_{\text{poly}}^2 aK_t k_C + 240\mu_{\text{poly}}^2 k_C\mu_C + 136\mu_{\text{poly}}^2 aK_t\mu_C + 176\mu_{\text{poly}}^2\mu_C^2 - 8\mu_{\text{poly}}\mu_C^3 + 9\mu_{\text{poly}} aK_t k_C\mu_C - 114\mu_{\text{poly}}\mu_C^2 k_C - 132\mu_{\text{poly}} aK_t\mu_C^2 - 57\mu_C^2 aK_t k_C - 4\mu_C^3 aK_t)\mu_{\text{poly}}/\mathcal{N} \quad (51)$$

$$A_{\text{in}} = 5(544\mu_{\text{poly}}^2 aK_t\mu_C + 192\mu_{\text{poly}}^2 aK_t k_C + 320\mu_{\text{poly}}^2\mu_C^2 + 1536\mu_{\text{poly}}^2 k_C\mu_C + 16\mu_{\text{poly}} aK_t\mu_C^2 + 228\mu_{\text{poly}} aK_t k_C\mu_C + 408ak_{\text{poly}}\mu_{\text{poly}} K_t\mu_C + 144ak_{\text{poly}}\mu_{\text{poly}} K_t k_C + 240k_{\text{poly}}\mu_{\text{poly}}\mu_C^2 + 1152k_{\text{poly}}\mu_{\text{poly}} k_C\mu_C + 12aK_t\mu_C^2 k_{\text{poly}} + 171aK_t k_C k_{\text{poly}}\mu_C)\mu_{\text{poly}}/\mathcal{N} \quad (52)$$

$$B_{\text{in}} = 240\mu_{\text{poly}}^2\mu_C(8\mu_{\text{poly}}\mu_C + 6k_{\text{poly}}\mu_C - 12\mu_{\text{poly}} k_C - 9k_{\text{poly}} k_C)/(a^2\mathcal{N}) \quad (53)$$

$$\mathcal{N} = 1408\mu_{\text{poly}}^3\mu_C^2 + 192\mu_{\text{poly}}^2\mu_C^3 + 24\mu_C^3 ak_{\text{poly}} K_t + 342\mu_C^2 ak_{\text{poly}} K_t k_C + 1920\mu_{\text{poly}}^3 k_C\mu_C + 1088\mu_{\text{poly}}^3\mu_C aK_t + 384\mu_{\text{poly}}^3 aK_t k_C + 1664a\mu_{\text{poly}}^2 K_t\mu_C^2 + 1584\mu_{\text{poly}}^2 k_{\text{poly}}\mu_C^2 + 1032a\mu_{\text{poly}}^2 K_t k_C\mu_C + 2160\mu_{\text{poly}}^2 k_{\text{poly}} k_C\mu_C + 2736\mu_{\text{poly}}^2\mu_C^2 k_C + 432\mu_{\text{poly}}^2 ak_{\text{poly}} K_t k_C + 1224\mu_{\text{poly}}^2 ak_{\text{poly}} K_t\mu_C + 801aK_t k_C k_{\text{poly}}\mu_{\text{poly}}\mu_C + 852aK_t\mu_C^2 k_{\text{poly}}\mu_{\text{poly}} + 1710\mu_{\text{poly}}\mu_C^2 k_{\text{poly}} k_C + 120\mu_{\text{poly}}\mu_C^3 k_{\text{poly}} + 684\mu_{\text{poly}}\mu_C^2 aK_t k_C + 48\mu_{\text{poly}}\mu_C^3 aK_t \quad (54)$$

They define the displacement fields (14) and (16), which give access to strains $\boldsymbol{\varepsilon} = \nabla^s\underline{\xi}$, stresses $\boldsymbol{\Sigma}$ (via $(12)_1$, and $(12)_3$ respectively), mean interface displacements $\bar{\underline{\xi}}$ and interface tractions $\underline{t}$ (via $(12)_2$).

## References


1. Akao M, Aoki H, Kato K (1981) J Mater Sci 16:809
2. Barthelat F, Tang H, Zavattieri PD, Li C-M, Espinosa HD (2007) J Mech Phys Solids 55(2):306
3. Barthélémy J-F, Dormieux L (2003) Comptes Rendus Mecanique 331:271
4. Barthélémy J-F, Dormieux L (2004) Int J Numer Anal Methods Geomech 28(7–8):565
5. Bernard O, Ulm FJ, Lemarchand E (2003) Cement Concr Res 33(9):1293
6. Bernaud D, Deudé V, Dormieux L, Maghous S, Schmitt DP (2002) Int J Numer Anal Methods Geomech 26:845
7. Chu T-MG, Orton DG, Hollister SJ, Feinberg SE, Halloran JW (2002) Biomaterials 23:1283
8. de With G, van Dijk HJA, Hattu N, Prijs K (1981) J Mater Sci 16:1592
9. Dormieux L (2005) In: Dormieux and Ulm [16], p 109
10. Dormieux L, Barthélémy J-F, Maghous S (2006) Comptes Rendus Mecanique 334:111, In French
11. Dormieux L, Kondo D, Ulm F-J (2006) Microporomechanics. Wiley
12. Dormieux L, Maghous S (2000) CR Acad Sci IIb – Math – Mech 328(8):593, In French
13. Dormieux L, Molinari A, Kondo D (2002) J Mech Phys Solids 50:2203
14. Dormieux L, Sanahuja J, Maalej Y (2007) Comptes Rendus Mecanique 335:25, In French
15. Dormieux L, Sanahuja J, Maghous S (2006) Comptes Rendus Mecanique 334:19
16. Dormieux L, Ulm F-J (eds) (2005) CISM courses and lectures, vol 480. Applied micromechanics of porous media. Springer, Wien
17. Eshelby JD (1957) Proc Roy Soc Lond, Ser A 241:376
18. Fritsch A, Dormieux L, Hellmich Ch (2006) Comptes Rendus Mécanique 334(3):151
19. Fritsch A, Hellmich Ch (2007) J Theor Biol 244(4):597
20. de Gennes P-G, Okumura K (2000) CR Acad Sci IV 1(2):257
21. Hashin Z (1991) J Appl Mech 58:444
22. Hellmich Ch, Barthélémy J-F, Dormieux L (2004) Eur J Mech A-Solids 23:783
23. Hellmich Ch, Mang HA (2005) J Mater Civil Eng (ASCE) 17(3):246
24. Hellmich Ch, Ulm F-J (2002) J Eng Mech (ASCE) 128(8):898
25. Hellmich Ch, Ulm F-J, Dormieux L (2004) Biomech Model Mechanobiol 2:219
26. Hench LL, Jones JR (eds) (2005) Biomaterials, artificial organs and tissue engineering. Woodhead Publishing, Cambridge, UK
27. Hervé E, Zaoui A (1993) Int J Eng Sci 31(1):1
28. Hill R (1963) J Mech Phys Solids 11:357
29. Hofstetter K, Hellmich Ch, Eberhardsteiner J (2005) Eur J Mech A – Solids 24(6):1030
30. Hofstetter K, Hellmich Ch, Eberhardsteiner J (2006) Comput Assisted Mech Eng Sci 13(4):523
31. Hunt BR, Eipsman RL, Rosenberg JM (2001) A guide to MATLAB for beginners and experienced users, 1st edn. Cambridge University Press, Cambridge, UK
32. Katti DR, Katti KS (2001) J Mater Sci 36(6):1411
33. Katti DR, Katti KS, Sopp JM, Sarikaya M (2001) Comput Theor Polym Sci 11(5):397–404
34. Katz JK, Ukraincik K (1971) J Biomech 4:221
35. Kreher W (1990) J Mech Phys Solids 38(1):115
36. LeGeros RZ (2002) Clin Orthop Relat Res 395:81
37. Lemarchand E, Ulm F-J, Dormieux L (2002) J Eng Mech (ASCE) 128(8):876
38. Martin RI, Brown PW (1995) J Mater Sci: Mater Med 6:138
39. Okumura K (2002) Eur Phys JE – Soft Matter 7(4):303
40. Okumura K (2003) Europhys Lett 63(5):701
41. Okumura K, de Gennes P-G (2001) The Eur Phys JE – Soft Matter 4(1):121
42. Peelen JGJ, Rejda BV, de Groot K (1978) Ceramurgia Int 4(2):71
43. Pramanik S, Agarwal AK, Rai KN, Garg A (2007) Ceram Int 33(3):419
44. Sanahuja J, Dormieux L (2005) Comptes Rendus Mecanique 333:818, In French
45. Schwefel H (1977) Numerische Optimierung von Computer-Modellen mittels der Evolutionsstrategie. Birkhäuser Basel, Switzerland, In German
46. Suchanek W, Yoshimura M (1998) J Mater Res 13(1):94
47. Suquet P (ed) (1997) Continuum micromechanics. Springer, Wien
48. Tai K, Ulm F-J, Ortiz Ch (2006) Nano Lett 6(11):2520

49. Ulm F-J, Constantinides G, Heukamp FH (2004) Materials and structures 37(1):43
50. Ulm F-J, Delafargue A, Constantinides G (2005) In: Dormieux and Ulm [16], p 207
51. Zaoui A (1997) In: Suquet [47], p 291
52. Zaoui A (2002) J Eng Mech (ASCE) 128(8):808
53. Zhong Z, Meguid SA (1997) J Elasticity 46(2):91